Turkish Journal of Chemistry

http://journals.tubitak.gov.tr/chem/

Research Article

Turk J Chem
(2021) 45: 377-386

doi:10.3906/kim-2008-34

Accelerated Fe^{III}/Fe^{II} redox cycle of Fenton reaction system using Pd/NH_2-MIL-101(Cr) and hydrogen

Zhong-Xing LIU[1], Xin LIU[1,2,*], Yong LI[1], Shi-Qian GAO[1]

[1]Institute of Environmental Protection Application Technology, School of Environmental Science and Engineering, Tianping College of Suzhou University of Science and Technology, Suzhou University of Science and Technology, Suzhou, Jiangsu Province, China
[2]Suzhou Mengli Environmental Technology Co., Ltd., Changshu National New & Hi-tech Industrial Development Zone Suzhou, Jiangsu Province, China

Received: 20.08.2020 • **Accepted/Published Online:** 13.12.2020 • **Final Version:** 28.04.2021

Abstract: In this paper, a novel improvement in the catalytic Fenton reaction system named MHACF-NH_2-MIL-101(Cr) was constructed based on H_2 and Pd/NH_2-MIL-101(Cr). The improved system would result in an accelerated reduction in Fe^{III}, and provide a continuous and fast degradation efficiency of the 10 mg L^{-1} 4-chlorophenol which was the model contaminant by using only trace level Fe^{II}. The activity of Pd/NH_2-MIL-101(Cr) decreased from 100% to about 35% gradually during the six consecutive reaction cycles of 18 h. That could be attributed to the irreversible structural damage of NH_2-MIL-101(Cr).

Key words: Fenton reaction, accelerated reduction of Fe^{III}, hydrogen, palladium, NH_2-MIL-101(Cr)

1. Introduction

The classic Fenton reaction has been widely applied in industrial wastewater treatment for the past 20 years because the refractory organics, such as phenols, aldehydes and halogenated hydrocarbons, could be efficiently degraded into low molecular weight organic acid, CO_2 and H_2O through this process under room temperature and normal pressure [1–5].

When the Fenton reaction is completed, the pH of effluent should be adjusted to 6~9 to meet the discharge quality of natural water. However, large amounts of iron sludge will be generated. That should be attributed to the ferrous salt that was continuously used to maintain the decomposition of hydrogen peroxide in order to produce hydroxyl radical (·OH).

Based on Equation (1) to (6) [6], more Fe^{III} will be produced in Fenton reaction. However, the regeneration of ferrous ions cannot be observed macroscopically. The iron sludge could not be reduced by incineration because it consisted of iron oxyhydroxides [7]. And it will take up lots of land if it is landfilled. Its proper disposal is closely related to the application and promotion of Fenton reaction in future. Thus, accelerating the reduction of Fe^{III} may be a useful method.

$$Fe^{II} + H_2O_2 \rightarrow \cdot OH + Fe^{III} + OH^- \quad (1)$$

$$Fe^{III} + H_2O_2 \rightarrow Fe^{II} + H^+ + HO_2^{\cdot} \quad (2)$$

$$Fe^{II} + \cdot OH \rightarrow OH^- + Fe^{III} \quad (3)$$

$$H_2O_2 + \cdot OH \rightarrow HO_2^{\cdot} + H_2O \quad (4)$$

$$Fe^{III} + HO_2^{\cdot} \rightarrow H^+ + Fe^{II} + O_2 \quad (5)$$

$$Fe^{II} + HO_2^{\cdot} + H^+ \rightarrow Fe^{III} + H_2O_2 \quad (6)$$

While previous studies utilised organic reductants like vitamin C, thioglycolic acid and tea polyphenols to achieve the above purpose [8–14], failure to control their quantity of accurately would result in a new organic pollution in effluent.

Granted there are many reductants, nevertheless, the use of hydrogen appears to the best choice due to it being an efficient inorganic reductant, the Fe^{III} could quickly be reduced by it without the problem of secondary organic pollution since its byproduct is just H_2O as shown in Equation (7) [15]. This led to the development of the accelerated catalytic Fenton (ACF) system through the introduction of hydrogen and Pd^0/Al_2O_3 into the classic Fenton system. The methyl tert-butyl ether could be continuously degraded using only1 mg L^{-1} Fe^{II} with the elimination of iron sludge [15,16].

$$[H] + [Fe(H_2O)_5(OH)]^{2+} \rightarrow [Fe(H_2O)_6]^{2+} \quad (7)$$

Most of them will return back to the atmosphere immediately after it is supplied into the water. Therefore, it should be maintained at 0.1 MPa hydrogen partial pressure during the whole process which will cause huge waste [15,16].

* Correspondence: liuxin0240357@126.com

With huge open metal sites and specific surface area, the metal-organic frameworks (MOFs) materials have gained more and more attention in the field of hydrogen storage [17–29], adsorption of pollutants [30–32], separation of gas component [33,34], monitoring pollutants [35,36] and hydrogen production [37,38]. And it could also be used as a carrier for noble metal catalysts, especially for Pd^0 [39–43].

In our previous study, the hydrogen combination with MOFs material was first proposed to accelerate the reduction of Fe^{III} in Fenton reaction. A novel MOFs-hydrogen-accelerated catalytic fenton (MHACF) system was constructed using MIL-101(Cr) as the carrier of Pd^0, leading to an extension in the retention time of H_2 in solution. ·OH could be continuously generated by using only trace amounts of ferrous ion in that system. Although the MIL-101(Cr) will be gradually damaged during the reaction process [44,45]. These two papers would serve as a basis for further studies on the subject matter, with particular concentration on the reduction of iron sludge in Fenton system, and how improvements can be on suitable catalytic materials.

In this paper, H_2 was still used to accelerate the Fe^{III}/Fe^{II} cycling in Fenton reaction. Pd^0, which is a common industrial catalyst and adsorbent and activator for hydrogen, (Equation (8)) [15,46] was chosen to enhance the retention of H_2 in aqueous solution. The NH_2-MIL-101(Cr), which could be stable in water and has acted as a novel material for hydrogen storage, applications in catalysis and the carrier for Pd^0 [47–56], was chosen to be used in this paper. The reaction mechanism of this novel MHACF-NH_2-MIL-101(Cr) system is depicted in Scheme 1.

$$2Pd + H_2 \rightarrow 2Pd\text{-}[H] \quad (8)$$

This work was to explore the cycling of Fe^{III}/Fe^{II}, and to investigate its degradation capacity and durability in this MHACF-NH_2-MIL-101(Cr) system.

2. Materials and methods

2.1. Materials

All the chemical reagents were purchased from China National Pharmaceutical Group Corporation. They were of analytical grade (purity ≥ 99.0%) and used without further purification. All the aqueous solutions were prepared by ultra-pure water (Millipore Milli-Q system, resistivity > 18.2 MΩ). Ferrous ion, ferric ion and 4-chlorophenol solution were prepared by dissolving iron(II) sulfate heptahydrate, iron(III) chloride (anhydrous) and 4-chlorophenol in ultra-pure water. The initial pH was adjusted by sulfuric acid and sodium hydroxide.

2.2. Synthetic procedures of the solid catalyst

The NH_2-MIL-101(Cr) was produced by this procedure [57]. 0.72 g 2-aminoterephthalic acid, 1.6 g chromic nitrate nonahydrate, and 0.4 g NaOH were dispersed in 30 mL ultra-pure water and stirred for at least 10 min. This solution was added into a Teflon lined stainless steel autoclave. After the operation mentioned above, it was placed in a preheated oven in the condition of 150 °C. After 12 h reaction process, it was naturally cooled to 20 °C room temperature. Then, this precipitate was recovered by centrifugation. It was alternately washed by using N,N dimethylformamide, hot absolute alcohol, and ultra-pure water three times in room temperature. After the operation mentioned above, the solid product was dried in the condition of 80 °C in DZF-6930 vacuum drying oven (Shanghai Bluepard Instruments Co., Ltd, China). And it was also activated 150 min in the condition of 150 °C before it was utilised in it.

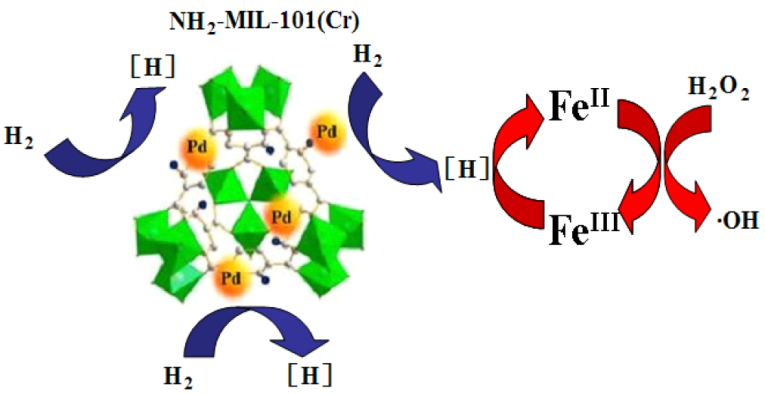

Scheme 1. The reaction mechanism of MHACF-NH_2-MIL-101(Cr) reaction system.

The Pd/NH_2-MIL-101(Cr) (Pd^0 0.5 wt% based on Agilent 720ES ICP-OES USA) was synthesised via a modification procedure, which was reported by Chen et al. [58]. 0.0188 g polyvinyl alcohol was dissolved in the condition of 95 °C. It was transferred into a three-necked flask, which contained 200 mg L^{-1} $PdCl_2$ solution after it was cooled to 20 °C. After vigorous agitation for 1 h, the freshly prepared $NaBH_4$ solution was drop wised into the flask. The Pd^0 was generated by the reduction of $PdCl_2$. The pH of aqueous solution was maintained at 7–8 by using HCl. Then 1 g activated MOFs material was added into the mixture immediately. It was agitated vigorously for 4 h. During the entire operation process, the whole flask was immersed into the ice-water mixture. Finally, the solid was collected and dried in the condition of 80 °C in a vacuum drying oven. It was also activated for 150 min in the same vacuum drying oven mentioned above in the condition of 150 °C before it was used in the reaction.

2.3. Characterisation of materials

All of the instruments used to characterise the materials including Fourier transform infrared spectroscopy (FT-IR), X-ray diffraction (XRD), Brunner-Emmet-Teller measurements (BET), X-ray photoelectron spectroscopy (XPS), scanning electron microscope (SEM) and transmission electron microscope (TEM) were same to those in our previous works [44,45].

2.4. The operation of the novel reaction system

The experiment was operated in a fume hood at normal temperature (20 ± 2 °C) and pressure. It was conducted in a 200 mL two-necked flat bottom flask equipped with magnetic stirrer. Before the experiment, the H_2 produced by hydrogen generator (Beijing BCHP Analytical Technology Institute, China) was continuously supplied more than 5min to eliminate dissolved oxygen. Its purity was more than 99.999%. After the H_2O_2 was added into the flask, the experiment began. The escaping hydrogen was collected by the pipeline and sent to the roof by the fan. There was no fire source within 300 m around the exhaust vent.

During the 6 consecutive reaction cycles, after the samples had been taken out at the end of each reaction cycle, H_2O_2 and 4-chlorophenol (4-CP) was immediately added into the system to maintain the initial concentration in the next reaction cycle at about 25 mM and 10 mg L^{-1}, respectively.

Water samples were taken out by disposable syringe and filtered immediately by hydrophilic polyethersulfone filters which had a pore size of 0.45 μm.

The filtrate was used for the concentration analysis of para-hydroxybenzoic acid (p-HBA), H_2O_2, 4-CP, ferrous ion, total Cr (Cr^{3+} and Cr^{6+}, abbreviated as TCr) and total Pd (abbreviated as TPd).

2.5. Methods of sample analysis

The instrument and methods for quantitative analysis of pH, ferrous, low molecular weight organic acid, TCr, TPd, H_2O_2, p-HBA and 4-CP are the same as previous study [7,44,45,59,60]. Quantitative analysis of p-Hydroxybenzoic acid (p-HBA) and 4-CP was performed with LC-20AT high performance liquid chromatography (Shimadzu, Japan) equipped with a reversed phase Agilent ZORBAX Eclipse XDB-C18 column (Agilent, USA) (4.6 mm × 150 mm, 5 μm). A SPD-M20A detector was used for the analysis. The concentration of Cl^- was measured by DIONEX ICS-900 (DIONEX, USA) coupled with a conductivity detector, IonPac AS23 Anion-Exchange Column and IonPac AG23 Guard Column (DIONEX, USA) at 24 °C. The eluent, containing 4.5 mM Na_2CO_3 + 0.8 mM $NaHCO_3$, was pumped at a flow rate of 1.0 mL min^{-1}. The suppresion current and injection volume were set to 46 mA and 10 μL, respectively. The concentration of iminodiacetate, formate and acetate was measured by DIONEX ICS-1100 (DIONEX, USA) coupled with a conductivity detector, IonPac AS11-HC anion-exchange column and IonPac® AG11-HC guard column at 24 °C. The eluent of KOH was pumped at a flow rate of 1.0 mL min^{-1}. The elution program was as follows: 0 ~ 17 min, 0.8 mM KOH; 17 ~ 52 min, 30 mM KOH; 52 ~ 55min, 0.8 mM KOH. The suppresion current and injection volume were set to 120 mA and 150 μL respectively. pH value was determined by pHS-3C pH meter (Shanghai Precision & Scientific Instrument Co. Ltd, Shangai, China). The error bars in all of the figures represented the standard deviation after three measurements

3. Results and discussion

3.1. Characterisation of the materials

The characterisation of the MOFs materials can be seen in the supplementary materal.

3.2. Transformation of iron valence in the reaction system

The transformation of iron valence in H_2 without using MOFs system, H_2-MOFs system, and H_2-Pd/MOFs system was shown in Figure 1(a). Ferrous ions could not be detected in the H_2 without using MOFs system. That means the reduction of Fe^{III} could be negligible because H_2 is insoluble in water. Ferrous ions increased from 0 to 21.78 μM, and to 2.26 μM in H_2-Pd/MOFs and H_2-MOFs systems respectively. This means Fe^{III} could be reduced by hydrogen. And the reduction of Fe^{III}

was enhanced significantly by using NH_2-MIL-101(Cr) and Pd^0 compared with that of the introduction of only NH_2-MIL-101(Cr). That means the retention time of H_2/[H] in aqueous solution was extended (Equation (8) and Equation (9)) [15].

$$Pd\text{-}[H] + Fe^{III} \rightarrow Pd + Fe^{II} + H^+ \quad (9)$$

As seen in Figure 1(b), the solution pH ranged from 2.9 to 3.05, showing that Equation (8) and Equation (9) existed in this system. Fe^{2+} decreased gradually from 24.96 μM to 13.94 μM. It decreased from 24.94 μM to 5.46 μM within five minutes after the start of the reaction in the classic Fenton system. Then it decreased gradually to 4.84 μM in the remaining 175 min. This means the reduction of Fe^{III} was enhanced by hydrogen in this novel system (Equation (1), Equation (3) and Equation (6)). Therefore, the degradation ability of MHACF-NH_2-MIL-101(Cr) could be improved using only trace amounts of Fe due to the rapid cycling of Fe^{III}/Fe^{II}.

3.3. Hydroxyl radicals in the system

The H_2O_2 in the novel system decreased from 25.06 mM to 2.35 mM in the first 5 min, as shown in Figure 2(a). Then, it decreased gradually to 1.98 μM in the remaining 175 min. Besides, the benzoic acid (BA) was used as the quencher of ·OH in this work. The quenched product was p-HBA [59]. The p-HBA increased rapidly from 0 to 87.39 μM after the whole reaction process. Therefore, it could be verified that the ·OH derived from the decomposition of H_2O_2 existed in this novel system.

3.4. The robustness of solid catalyst in the system

As a raw material for disinfectants, leather preservatives and insecticides, the 4-CP is one of representative refractory organic pollutant in both developing and developed countries but due to it being a toxic pollutant, it is banned in developed countries [61,62]. In this paper, it was chosen as the model contaminant. Previous studies showed that direct oxidation and stripping of O_2, and the coagulation sedimentation of iron salt could be negligible in the removal of 4-CP, while it could be rapidly degraded in the Fenton system [7].

Results obtained in Figure 2(b) shows that in the 1st reaction cycle of the classic Fenton reaction, 4-CP could be degraded thoroughly, though the degradation efficiency in the 2nd 3h reaction cycle rapidly decreases to 8.5%. The degradation efficiency maintained this downward trend in the rest 4 cycles. The degradation efficiency was less than 1% after completing the whole 6 reaction cycles. From Equation(1) to Equation(6), the ·OH was insufficient in the 2nd, 3rd, 4th, 5th and 6th cycle. This may be attributed to the faster consumption and slower regeneration of Fe^{II}.

In contrast, 4-CP could be eliminated thoroughly in 120 min in the 1st reaction cycle of MHACF-NH_2-MIL-101(Cr) system and it could maintain more than 35% degradation efficiency after 6 consecutive reaction cycles by using only

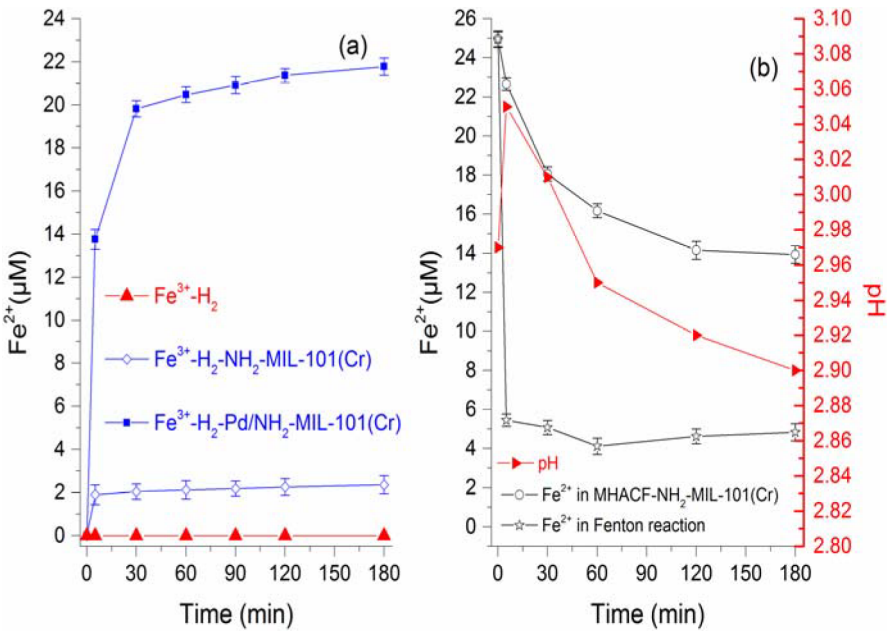

Figure 1. (a) Variation of ferrous ion in Fe^{3+}-H_2-Pd/NH_2-MIL-101(Cr), Fe^{3+}-H_2-MIL-101(Cr), and Fe^{3+}-H_2 system, respectively (the initial aqueous solution pH was about 2.5); (b) variation of pH and ferrous ion in MHACF-NH_2-MIL-101(Cr) system, and variation of ferrous ion in Fenton system. Except for the parameters investigated, other initial parameters were NH_2-MIL-101(Cr) 2 g L^{-1}, Fe^{3+} 25 μM, H_2 85 mL min^{-1}, H_2O_2 25 mM, Pd/NH_2-MIL-101(Cr) 2 g L^{-1}, Fe^{2+} 25 μM and initial pH 3.

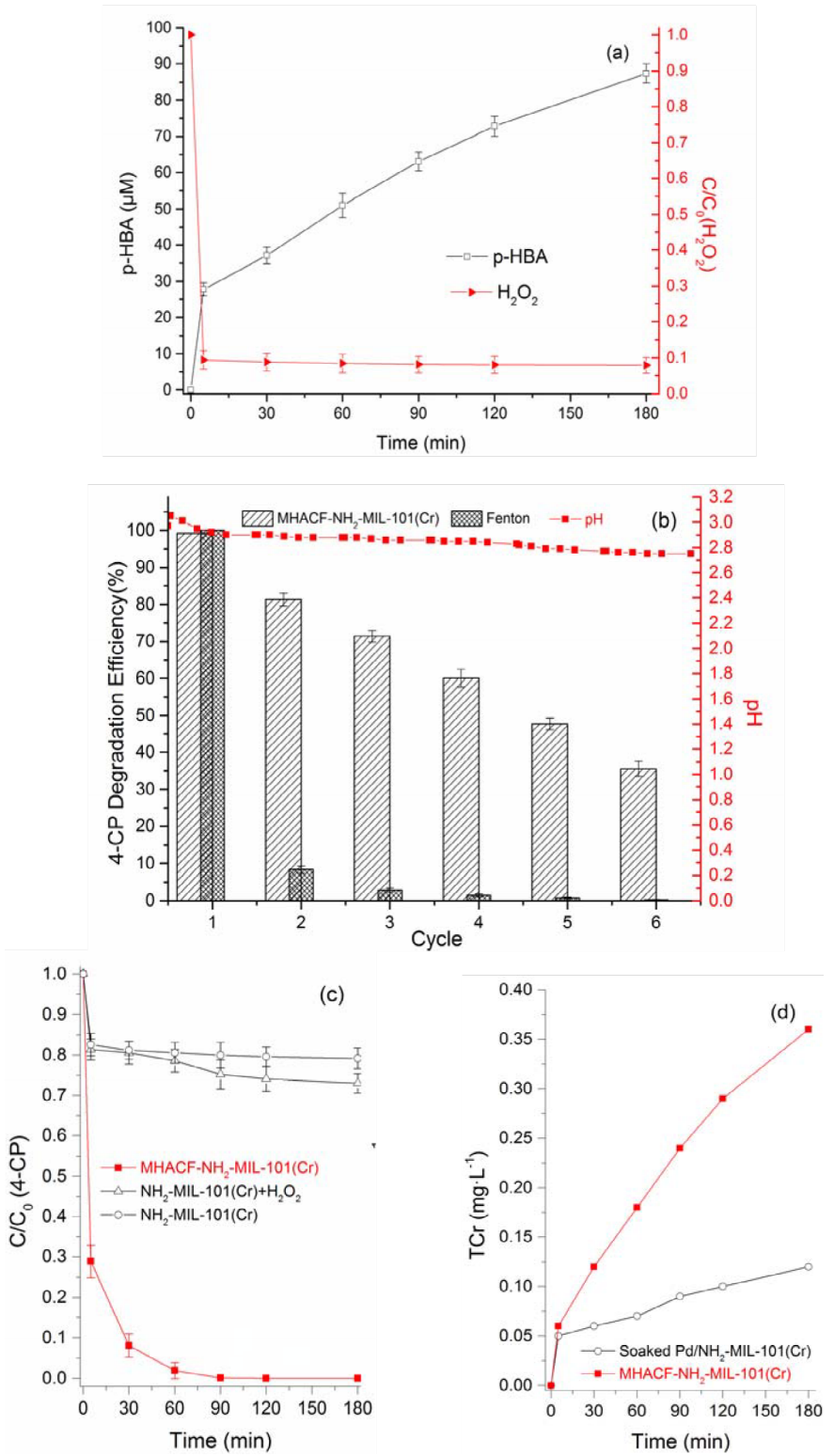

Figure 2. (a) Variation of p-HBA and H_2O_2 in MHACF-NH_2-MIL-101(Cr) system (BA was used as ·OH scavenger); (b) 4-CP degradation efficiency of 6 consecutive reaction cycles in Fenton and MHACF-NH_2-MIL-101(Cr) system, respectively. Variation of pH in MHACF-NH_2-MIL-101(Cr) during 6 consecutive reaction cycles (each reaction cycle was 180 min); (c) the control test of 4-CP; (d) variation of TCr in H_2SO_4 solution (without H_2, 4-CP, Fe^{2+} and H_2O_2) and MHACF-NH_2-MIL-101(Cr) system (without 4-CP), respectively. Except for the parameters investigated, other initial parameters were BA 1.8 g·L^{-1}, Fe^{2+} 25 μM, H_2O_2 25 mM, Pd/NH_2-MIL-101(Cr) 2 g L^{-1}, H_2 85 mL min^{-1}, and pH 3.

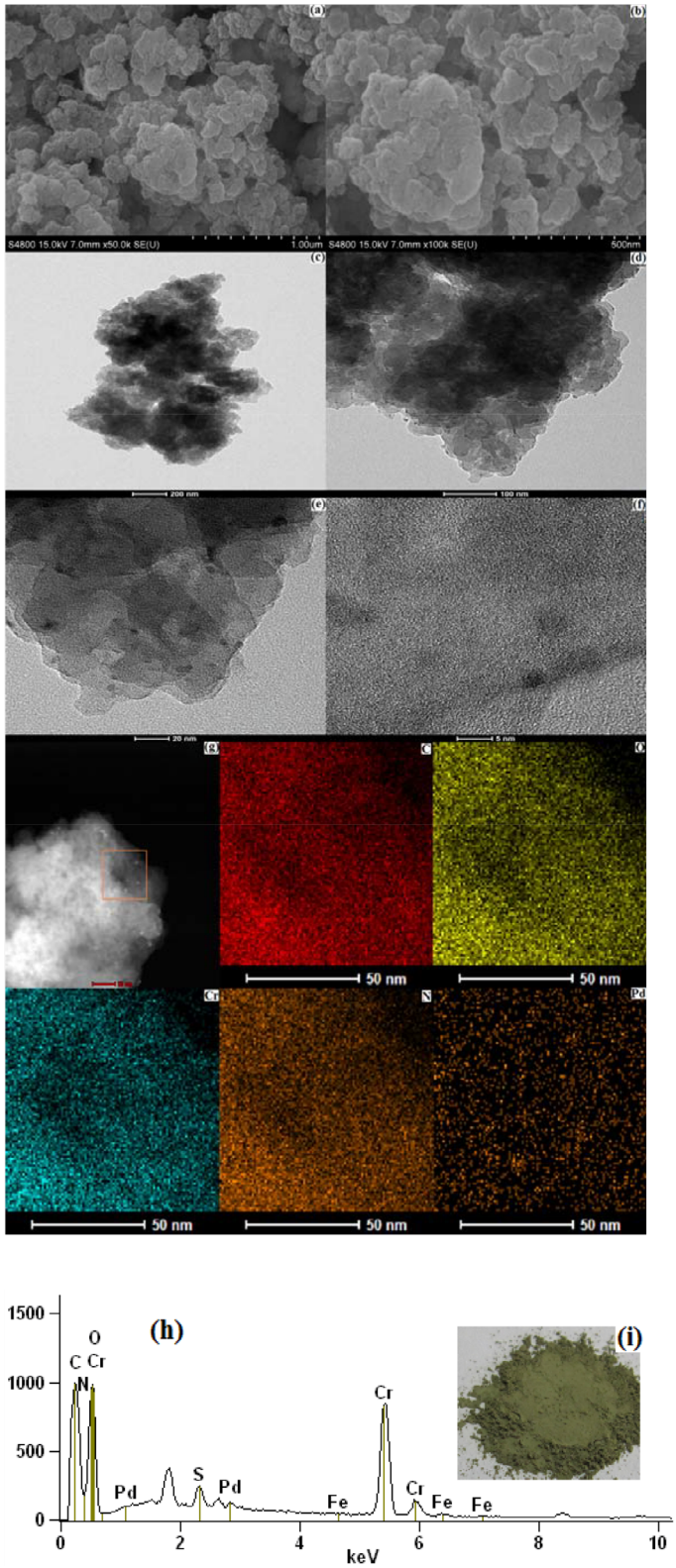

Figure 3. Characterisation of the residue in MHACF-NH_2-MIL-101(Cr) system after 6 consecutive reaction cycles (without 4-CP): (a) the SEM photograph (1 μm scale); (b) the SEM photograph (500 nm scale); (c) the TEM photograph (200 nm scale); (d) The TEM photograph (100 nm scale); (e) the TEM photograph (20 nm scale); (f) the TEM photograph (5 nm scale); (g) element mappings images; (h) the EDX photograph; (i) the appearance of residue. Each reaction cycle was 180 min.

trace amount of Fe^{II}/Fe^{III}. It means ·OH was comparatively sufficient during the whole 6 reaction cycles and this could be attributed to the faster regeneration of Fe^{II} accelerated by using hydrogen and Pd/NH_2MIL-101(Cr) (Equation(8), Equation(9)) [15].

The pH gradually decreases from 2.97 at the beginning of the reaction to 2.75 after 6 consecutive reaction cycles. This phenomenon reflects the fact that the Fe^{II} regenerated rapidly by the reduction of Fe^{III} (Equation (9)).

In the 1st cycle of this novel system, 0.56 mg L^{-1} 4-chlorobenzene-1,2-diol and 0.47 mg L^{-1} cis-2-butenedioic acid was detected at 110 min., 0.42 mg L^{-1} cis-2-butenedioic acid was detected at 160 min. The p-benzoquinone and hydroquinone could not be detected. This result was similar to findings from other studies [7,44,45,63].

Phenols could be removed by the adsorption process of MOFs [64]. According to the BET test, the specific surface area of NH_2-MIL-101(Cr), before it was utilised in the reaction, was 1698.99 m^2 g^{-1}. Less than 20% 4-CP could be removed by the adsorption of MOFs, as shown in Figure 2(c). The difference in removal efficiency between NH_2-MIL-101(Cr) system and NH_2-MIL-101(Cr) + H_2O_2 system was not significant. The generation of ·OH in NH_2-MIL-101(Cr) + H_2O_2 system could be negligible. Therefore, the role of this MOFs material in the MHACF-NH_2-MIL-101(Cr) system was hydrogen storage material and carrier of Pd^0.

As shown in Figure 2(b), the degradation efficiency in MHACF-NH_2-MIL-101(Cr) system was 100% (1st cycle), 81.32% (2nd cycle), 71.42% (3rd cycle), 60.08% (4th cycle), 47.48% (5th cycle) and 35.62% (final cycle), respectively. Combined with the results depicted in Figure 2(d), the TCr increased gradually from 0 to 0.36 mg·L^{-1} during the 180 min reaction. The variation of TCr in H_2SO_4 aqueous solution was similar with our previous work [44,45]. The Pd was not detected in both solutions. Based on these results, it could be speculated that NH_2-MIL-101(Cr) was damaged gradually after the long-term operation of this novel system.

As revealed in Figure 3, the morphological change in Pd/NH_2-MIL-101(Cr) provided further direct evidence. As depicted in Figure 3(h), Figure 3(g) and Figure S2, the EDX spectrum, the element mapping images and the XPS signal intensiveness of the dark yellow green powder (shown in Figure 3(i)) which was the residue collected after the 6 reaction cycles, revealed that the C, N, Cr and Pd were still distributed in it, while its surface area was lower to only 841.71 m^2 g^{-1}. The results displayed in Figures 3(a) and 3(b) shows that the average diameter of single Pd/NH_2-MIL-101(Cr) particle was less than 300 nm. The appearance of the particles was more irregular compared with that exhibited in Figure S6(a) and Figure S6(b). Figure 3(c) to Figure 3(f) shows an octahedral structure which is the representative octahedral structure of NH_2-MIL-101(Cr) was not present in the residue when compared to what is exhibited in Figure S6(c) to Figure S6(f). Also, according to the XRD pattern of the residue shown in Figure S4(d), the intensiveness of the detection signal was significantly weaker after the 6 cycle reactions. Furthermore, according to XPS spectrum of Pd element depicted in Figure S3(d), the intensiveness of the residue increased significantly. This may be attributed to the Pd^0 loaded on the surface of this MOFs material being shed off during the reaction with the structural damage of NH_2-MIL-101(Cr) and the reduction of surface area, and then was gathered in aqueous solution. It was similar to our previous research results from MHACF-MIL-101(Cr) [44,45]. As established by the hard/soft acid/base principle, a more stable framework could be formed by high-valent metal cations by stronger coordination bonds. MOFs containing a higher oxidation state metal or a metal clusters tend to be more stable in acids due to the stronger coordination bonds [65,66]. Therefore, the MOFs consisting of the group 4 metal cations of the periodic table may be a new research direction.

4. Conclusion

With using trace amount of ferrous salt, the oxidative degradation capacity of novel MHACF-NH_2-MIL-101(Cr) system was much higher than that of Fenton system under normal pressure and temperature. The regeneration of Fe^{II} could be significantly accelerated by using hydrogen gas and solid catalyst Pd/NH_2-MIL-101(Cr). Under the premise that the hydroxyl radical could be continuously produced in this novel system, the yield of iron sludge could be reduced. However, the structure of NH_2-MIL-101(Cr) would be damaged in acidic condition which led to the leaching of chromium ions. In the future, more stable MOFs materials for the storage and activation of hydrogen are recommended to solve the above questions thoroughly. The idea behind this novel system offers new way for the research and development of significantly improved the application of Fenton reaction. This work is the beginning of a series of research work in future. We hope that scholars and engineers could focus on the improvement of Fenton reaction and explore and improve the suitable catalytic materials.

Acknowledgements

The author(s) disclosed receipt of the financial support for the research, authorship, and/or publication of this article. This work has been financially supported by the Natural Science Foundation of Jiangsu Province (NO.BK20160359),

Major Science and Technology Program for Water Pollution Control and Treatment (NO.2017ZX07205-02), Science and Technology Innovation and Entrepreneurship Leadership Talent Program of Changshu (NO.CSRC1708), Tianping College Student Innovation and Entrepreneurship Training Program of Suzhou University of Science and Technology (NO.2018029), Scientific Research Foundation of Suzhou University of Science and Technology (NO.341410031), and State Key Laboratory of Pollution Control and Resource Reuse Foundation (NO.PCRRF16027).

References

1. Bautista P, Mohedano A, Casas J, Zazo J, Rodriguez J. An overview of the application of fenton oxidation to industrial wastewaters treatment. Journal of Chemical Technology & Biotechnology 2008; 83: 1323-1338.
2. Guo S, Yuan N, Zhang G, Yu J. Graphene modified iron sludge derived from homogeneous fenton process as an efficient heterogeneous fenton catalyst for degradation of organic pollutants. Microporous and Mesoporous Materials 2017; 238: 62-68.
3. Zhang Y, Zhou M. A critical review of the application of chelating agents to enable fenton and fenton-like reactions at high pH values. Journal of hazardous materials 2019; 362: 436-450.
4. Monteil H, Péchaud Y, Oturan N, Oturan M. A review on efficiency and cost effectiveness of electro-and bio-electro-fenton processes: application to the treatment of pharmaceutical pollutants in water. Chemical Engineering Journal 2019; 376: 119577.
5. Hou J, Chen Z, Gao J, Xie Y, Li L et al. Simultaneous removal of antibiotics and antibiotic resistance genes from pharmaceutical wastewater using the combinations of up-flow anaerobic sludge bed, anoxic-oxic tank, and advanced oxidation technologies. Water Research 2019; 159: 511-520.
6. Liu X, Fan J, Ma L. Elimination of 4-chlorophenol in aqueous solution by the bimetallic Al–Fe/O_2 at normal temperature and pressure. Chemical Engineering Journal 2014; 236: 274-284.
7. Deng Y, Englehardt J. Treatment of landfill leachate by the Fenton process. Water Research 2006; 40: 3683-3694.
8. Huang X, Hou X, Jia F, Song F, Zhao J et al. Ascorbate-promoted surface iron cycle for efficient heterogeneous fenton alachlor degradation with hematite nanocrystals. ACS Applied Materials & Interfaces 2017; 9: 8751-8758.
9. Subramanian G, Madras G. Remarkable enhancement of fenton degradation at a wide pH range promoted by thioglycolic acid. Chemical Communications 2017; 53: 1136-1139.
10. Ouyang Q, Kou F, Zhang N, Lian J, Tu G et al. Tea polyphenols promote fenton-like reaction: pH self-driving chelation and reduction mechanism. Chemical Engineering Journal 2019; 366: 514-522.
11. Porras J, Giannakis S, Torres-Palma R, Fernandez J, Bensimon M et al. Fe and Cu in humic acid extracts modify bacterial inactivation pathways during solar disinfection and photo-fenton processes in water. Applied Catalysis B: Environmental 2018; 235: 75-83.
12. Li X, Guo W, Liu Z, Wang R, Liu H. Quinone-modified NH_2-MIL-101 (Fe) composite as a redox mediator for improved degradation of bisphenol A. Journal of hazardous materials 2017; 324: 665-672.
13. Yang Z, Yu A, Shan C, Gao G, Pan B. Enhanced Fe(III)-mediated fenton oxidation of atrazine in the presence of functionalized multi-walled carbon nanotubes. Water Research 2018; 137: 37-46.
14. Pan Y, Su H, Zhu Y, Molamahmood H, Long M. CaO_2 based fenton-like reaction at neutral pH: accelerated reduction of ferric species and production of superoxide radicals. Water Research 2018; 145: 731-740.
15. Georgi A, Polo M, Crincoli K, Mackenzie K, Kopinke F. Accelerated catalytic Fenton reaction with traces of iron: an Fe–Pd-multicatalysis approach. Environmental Science & Technology 2016; 50: 5882-5891.
16. Liang Y, Pan X, Zhang C, Xie, B, Liu, S. The simulation and analysis of leakage and explosion at a renewable hydrogen refuelling station. International Journal of Hydrogen Energy 2019; 44: 22608-22619.
17. Taylor M, Runčevski T, Oktawiec J, Bachman J, Siegelman R et al. Near-perfect CO_2/CH_4 selectivity achieved through reversible guest templating in the flexible metal–organic framework Co (bdp). Journal of the American Chemical Society 2018; 140: 10324-10331.
18. Li J, Duan Q, Wu Z, Li X, Chen K et al. Few-layered metal-organic framework nanosheets as a highly selective and efficient scavenger for heavy metal pollution treatment. Chemical Engineering Journal 2020; 383: 123189.
19. Zhang J, Sun L, Chen C, Liu M, Dong W et al. High performance humidity sensor based on metal organic framework MIL-101(Cr) nanoparticles. Journal of Alloys and Compounds 2017; 695: 520.
20. Li Y, Xiao A, Zou B, Zou B, Zhang H et al. Advances of metal–organic frameworks for gas sensing. Polyhedron 2018; 154: 83-97.
21. Kustov L, Isaeva V, Přech J, Bisht K. Metal-organic frameworks as materials for applications in sensors. Mendeleev Communications 2019; 29: 361-368.

22. Park H, Dincă M, Román-Leshkov Y. Continuous-flow production of succinic anhydrides via catalytic β-lactone carbonylation by Co (CO) 4⊂ Cr-MIL-101. Journal of the American Chemical Society, 2018; 140: 10669-10672.

23. Leszczyński M, Kornowicz A, Prochowicz D, Justyniak I, Noworyta K, et al. Straightforward synthesis of single-crystalline and redox-active Cr (II)-carboxylate MOFs. Inorganic chemistry *2018; 57:* 4803-4806.

24. Chen H, He Y, Pfefferle L, Pu W, Wu Y et al. Phenol Catalytic hydrogenation over palladium nanoparticles supported on metal-organic frameworks in the aqueous phase. ChemCatChem *2018; 10:* 2558-2570.

25. Vinogradov V, Drozdov A, Mingabudinova L, Shabanova E, Kolchina N et al. Composites based on heparin and MIL-101(Fe): the drug releasing depot for anticoagulant therapy and advanced medical nanofabrication. Journal of Materials Chemistry B 2018; 6: 2450-2459.

26. Kim S, Park C, Huh B, Lee S, Min C et al. Metal-organic frameworks, NH_2-MIL-88 (Fe), as carriers for ophthalmic delivery of brimonidine. Acta Biomaterialia 2018; 79: 344-353.

27. Wang H, Chen Y, Wang H, Liu X, Zhou X et al. DNAzyme-loaded metal-rrganic frameworks (MOFs) for self-sufficient gene therapy. Angewandte Chemie International Edition 2019; 58: 7380-7384.

28. Li X, Yang X, Xue H, Pang H, Xu Q. Metal–organic frameworks as a platform for clean energy applications. EnergyChem 2020; 2: 100027.

29. Chanchetti L, Leiva D, Faria L, Ishikawa T. A scientometric review of research in hydrogen storage materials. International Journal of Hydrogen Energy 2020; 45: 5356-5366.

30. Zhao J, Xu L, Su Y, Yu H, Liu H et al. Zr-MOFs loaded on polyurethane foam by polydopamine for enhanced dye adsorption. Journal of Environmental Sciences 2021; 101: 177-188.

31. Zhao C, Xu Y, Xiao F, Ma J, Zou Y et al. Perfluorooctane sulfonate removal by metal-organic frameworks (MOFs): insights into the effect and mechanism of metal nodes and organic ligands. Chemical Engineering Journal 2021; 406: 126852.

32. Esrafili L, Firuzabadi F, Morsali A, Hu M et al. Reuse of predesigned dual-functional metal organic frameworks (DF-MOFs) after heavy metal removal. Journal of Hazardous Materials 2021; 403: 123696.

33. Yu C, Ding Q, Hu J, Wang Q, Cui X et al. Selective capture of carbon dioxide from humid gases over a wide temperature range using a robust metal–organic framework. Chemical Engineering Journal 2021; 405: 126937.

34. Wang Q, Meng L, Chen H, Zhang Z, Xu D et al. Selective CO_2 or CH_4 adsorption of two anionic bcu-MOFs with two different counterions: experimental and simulation studies. Inorganic Chemistry Frontiers 2020; Advance Article.

35. Habila M, Alhenaki B, El-Marghany A, Sheikh M, Ghfar A et al. Metal organic frameworks enhanced dispersive solid phase microextraction of malathion before detection by UHPLC-MS/MS. Journal of Separation Science 2020; 43: 3103-3109.

36. Zhang Y, Liu J, Wu X, Tao W, Li Z. Ultrasensitive detection of Cr(VI) ($Cr_2O_7^{2-}$/CrO_4^{2-}) ions in water environment with a fluorescent sensor based on metal-organic frameworks combined with sulfur quantum dots. Analytica Chimica Acta 2020; 1131: 68-79.

37. Veeramani V, Matsagar B, Yamauchi Y, Badjah A, Naushad M et al. Metal organic framework derived nickel phosphide/graphitic carbon hybrid for electrochemical hydrogen generation reaction. Engineers 2019; 634-638.

38. Liu S, Zhang C, Sun Y, Chen Q, He L et al. Design of metal-organic framework-based photocatalysts for hydrogen generation. Coordination Chemistry Reviews 2020; 413: 213266.

39. Yuan N, Pascanu V, Huang Z, Valiente A, Heidenreich N et al. Probing the evolution of palladium species in Pd@MOF catalysts during the heck coupling reaction: an operando X-ray absorption spectroscopy study. Journal of the American Chemical Society 2018; 140: 8206-8217.

40. Niu H, Zheng Y, Wang S, Zhao L, Yang S et al. Continuous generation of hydroxyl radicals for highly efficient elimination of chlorophenols and phenols catalyzed by heterogeneous Fenton-like catalysts yolk/shell Pd@Fe_3O_4@metal organic frameworks. Journal of Hazardous Materials 2018; 346: 174-183.

41. Alamgholiloo H, Zhang S, Ahadi A, Rostamnia S, Banaei R et al. Synthesis of bimetallic 4-PySI-Pd@ Cu(BDC) via open metal site Cu-MOF: effect of metal and support of Pd@Cu-MOFs in H_2 generation from formic acid. Molecular Catalysis 2019; 467: 30-37.

42. Malouche A, Zlotea C, Szilágyi P. Interactions of hydrogen with Pd@ MOF composites. ChemPhysChem 2019; 20: 1282-1295.

43. Alamgholiloo H, Rostamnia S, Hassankhani A, Liu X, Eftekhari A et al. Formation and stabilization of colloidal ultra-small palladium nanoparticles on diamine-modified Cr-MIL-101: synergic boost to hydrogen production from formic acid. Journal of Colloid and Interface Science 2020; 567: 126-135.

44. Liu X, Gao S, Fan J, Li X, Qin H et al. The construction of accelerated catalytic Fenton reaction based on Pd/MIL-101(Cr) and H_2. New Journal of Chemistry 2019; 43: 8179-8188.

45. Liu X, Fan J, Liu Z, Yu Y, You J et al. Elimination of 4-chlorophenol in aqueous solution by the novel Pd/MIL-101(Cr)-hydrogen-accelerated catalytic fenton system. Applied Organometallic Chemistry 2019; 33: e5194.

46. Lou Z, Xu J, Zhou J, Yang K, Cao Z et al. Insight into atomic H* generation, H_2 evolution, and cathode potential of MnO_2 induced Pd/Ni foam cathode for electrocatalytic hydrodechlorination. Chemical Engineering Journal 2019; 374: 211-220.

47. Hassan H, Betiha M, Mohamed S, El-Sharkawy E, Ahmed E. Salen-Zr(IV) complex grafted into amine-tagged MIL-101(Cr) as a robust multifunctional catalyst for biodiesel production and organic transformation reactions. Applied Surface Science 2017; 412: 394-404.

48. Saikia M, Kaichev V, Saikia L. Gold nanoparticles supported on nanoscale amine-functionalized MIL-101(Cr) as a highly active catalyst for epoxidation of styrene. RSC advances 2016; 6: 106856-106865.

49. Lee Y, Yu K, Ravi S, Ahn W. Selective adsorption of rare earth elements over functionalized Cr-MIL-101. ACS applied materials & interfaces 2018; 10: 23918-23927.

50. Gaikwad S, Kim S, Han S. CO_2 capture using amine-functionalized bimetallic MIL-101 MOFs and their stability on exposure to humid air and acid gases. Microporous and Mesoporous Materials 2019; 277: 253-260.

51. Xie F, Zhang N, Zhuo L, Qin P, Chen S et al. "MOF-cloth" formed via supramolecular assembly of NH_2-MIL-101(Cr) crystals on dopamine modified polyimide fiber for high temperature fume paper-based filter. Composites Part B: Engineering 2019; 168: 406-412.

52. Lawson S, Griffin C, Rapp K, Rownaghi A, Rezaei F. Amine-functionalized MIL-101 monoliths for CO_2 removal from enclosed environments. Energy & Fuels 2019; 33: 2399-2407.

53. Wen M, Mori K, Kamegawa T, Yamashita H. Amine-functionalized MIL-101(Cr) with imbedded platinum nanoparticles as a durable photocatalyst for hydrogen production from water. Chemical Communications 2014; 50: 11645-11648.

54. Zhong R, Yu X, Meng W, Liu J, Zhi C et al. Amine-grafted MIL-101 (Cr) via double-solvent incorporation for synergistic enhancement of CO_2 uptake and selectivity. ACS Sustainable Chemistry & Engineering 2015; 6: 16493-16502.

55. Berenguer-Murcia Á, Marco-Lozar J. Cazorla-Amorós D. Hydrogen storage in porous materials: status, milestones, and challenges. The Chemical Record 2018; 18: 900-912.

56. García-Holley P, Schweitzer B, Islamoglu T, Liu Y, Lin L et al. Benchmark study of hydrogen storage in metal–organic frameworks under temperature and pressure swing conditions. ACS Energy Letters 2018; 3: 748-754.

57. Ma J, Ying Y, Guo X, Huang H, Liu D et al. Fabrication of mixed-matrix membrane containing metal–organic framework composite with task-specific ionic liquid for efficient CO_2 separation. Journal of Materials Chemistry A 2016; 4: 7281-7288.

58. Chen J, Liu R, Guo Y, Chen L, Gao H. Selective hydrogenation of biomass-based 5-hydroxymethylfurfural over catalyst of palladium immobilized on amine-functionalized metal–organic frameworks. Acs Catalysis 2014; 5: 722-733.

59. Pang S, Jiang J, Ma J. Oxidation of sulfoxides and arsenic (III) in corrosion of nanoscale zero valent iron by oxygen: evidence against ferryl ions (Fe(IV)) as active intermediates in Fenton reaction. Environmental science & technology 2011; 45: 307-312.

60. Nogueira R, Oliveira M, Paterlini W. Simple and fast spectrophotometric determination of H_2O_2 in photo-Fenton reactions using metavanadate. Talanta 2005; 66: 86-91.

61. Zhong W, Wang D, Wang Z. Distribution and potential ecological risk of 50 phenolic compounds in three rivers in Tianjin, China. Environmental Pollution 2018; 235: 121-128.

62. Munoz M, Pedro Z, Casas J, Rodriguez J. Assessment of the generation of chlorinated byproducts upon fenton-like oxidation of chlorophenols at different conditions. Journal of Hazardous Materials 2011; 190: 993-1000.

63. Zhou T, Li Y, Ji J, Wong F, Lu X. Oxidation of 4-chlorophenol in a heterogeneous zero valent iron/H_2O_2 fenton-like system: kinetic, pathway and effect factors. Separation and Purification Technology 2008; 62: 551-558.

64. Liu B, Yang F, Zou Y, Peng Y. Adsorption of phenol and p-nitrophenol from aqueous solutions on metal–organic frameworks: effect of hydrogen bonding. Journal of Chemical & Engineering Data 2014; 59: 1476-1482.

65. Wang K, Huang H, Xue W, Liu D, Zhao X et al. An ultrastable Zr metal–organic framework with a thiophene-type ligand containing methyl groups. CrystEngComm 2015; 17: 3586-3590.

66. Yuan S, Qin J, Lollar C, Zhou H. Stable metal–organic frameworks with group 4 metals: current status and trends. ACS central science 2018; 4: 440-450.

Supplementary Material

Characterisation of the Pd/NH_2-MIL-101(Cr)

As seen in Figure S1(a), the synthesised NH_2-MIL-101(Cr) was a yellowish-green powder. According to the FT-IR spectrum depicted in Figure S1(b), the peak at 3488 cm^{-1} corresponds to the stretching vibration of the asymmetric amino-group on phenyl ring. And the peak at 3365 cm^{-1} corresponds to the stretching vibration of the symmetric amino-group on phenyl ring. The peaks at 2928 cm^{-1} corresponds to the stretching vibration of the carbon-hydrogen on phenyl ring. The peaks at 1586 cm^{-1} corresponds to the nitrogen-hydrogen deformation. The peaks at 1497 cm^{-1} corresponds to the oxygen-carbon-oxygen stretching vibrations. The peaks at 1256 cm^{-1} corresponds to carbon-nitrogen stretching vibrations. The peaks at 766 cm^{-1} corresponds to symmetric stretching of disubstituted benzene. The peaks at 576 cm^{-1} correspond to the symmetric stretching of chromium-oxygen. According to the EDX and XPS spectrums of this MOFs material shown in Figure S2(g) and Figure S3(a) to Figure S3(c), it was revealed that the C, N, and Cr was distributed in the material. Its surface area was 1698.99 $m^2\ g^{-1}$, analysed by BET test. It was similar to the results on the synthesis of NH_2-MIL-101(Cr) reported by other scholars [1–4].

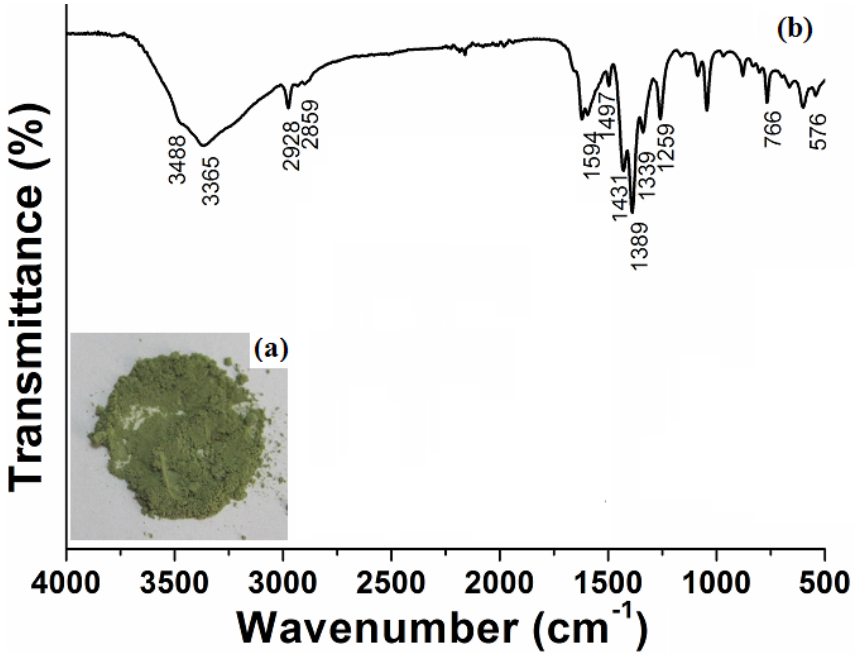

Figure S1. (a) The appearance and (b) FT-IR spectra of synthesised NH_2-MIL-101(Cr).

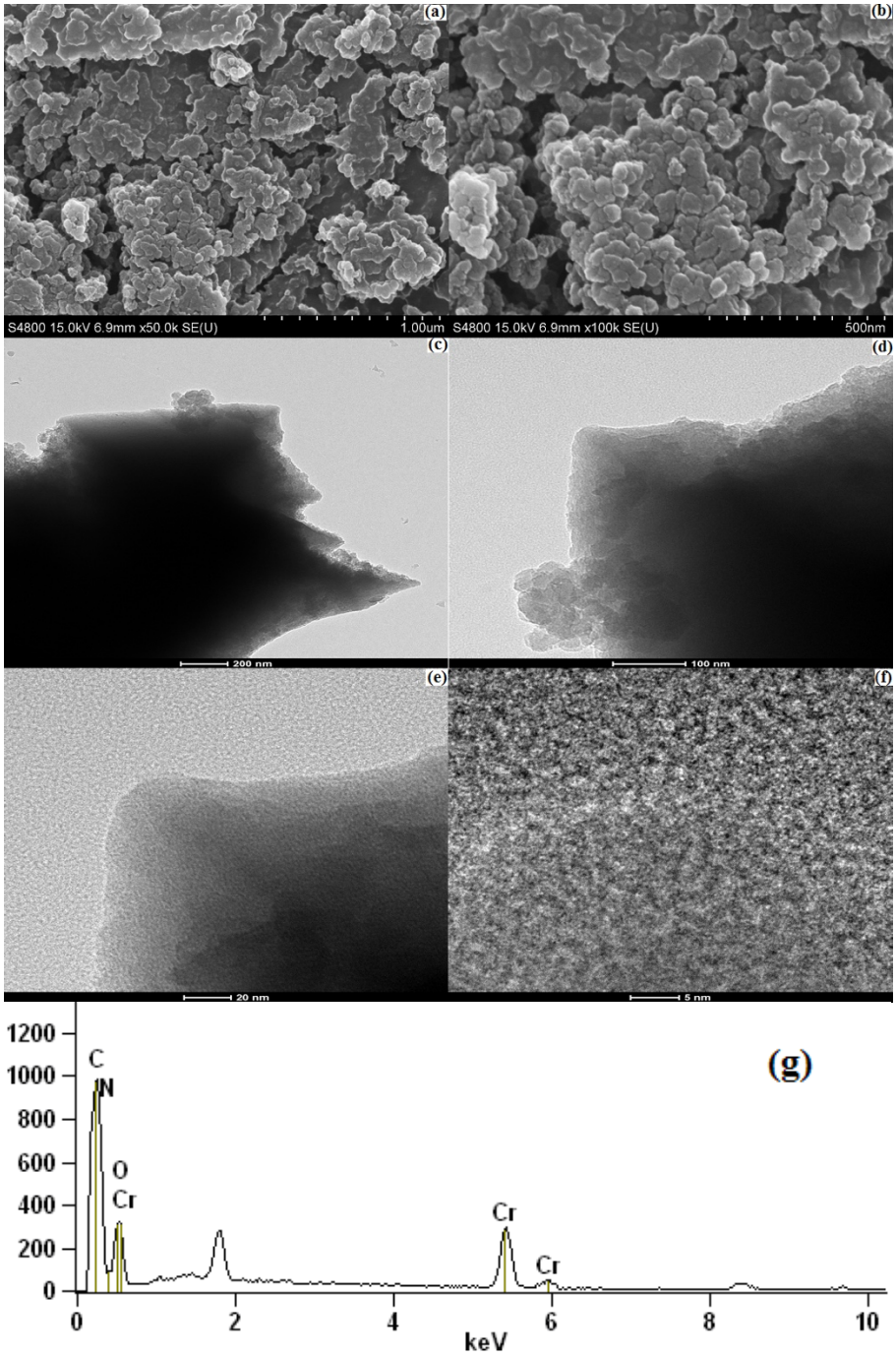

Figure S2. (a) The SEM photograph of NH_2-MIL-101(Cr) (1 μm scale); (b) the SEM photograph of NH_2-MIL-101(Cr) (500 nm scale); (c) the TEM photograph of NH_2-MIL-101(Cr) (200 nm scale); (d) the TEM photograph of NH_2-MIL-101(Cr) (100 nm scale); (e) the TEM photograph of NH_2-MIL-101(Cr) (20 nm scale); (f) the TEM photograph of NH_2-MIL-101(Cr) (5 nm scale); (g) the EDX photograph of NH_2-MIL-101(Cr))**.**

As seen in the SEM photographs of synthesised NH_2-MIL-101(Cr) shown in Figure S2(a) and Figure S2(b), the rough crystal morphology of the sample was in a relatively regular octahedron particle structure. The crystal particle was about 250–350 nm. It was in accordance with the results reported by Tian et al. [2], Zhang et al. [5], and Luo et al. [6]. According to the TEM images shown in Figure S2(c) to Figure S2(f), the edges of NH_2-MIL-101(Cr) could be observed.

The XRD of NH_2-MIL-101(Cr), shown in Figure S4 was similar to that of previous works [1–6].

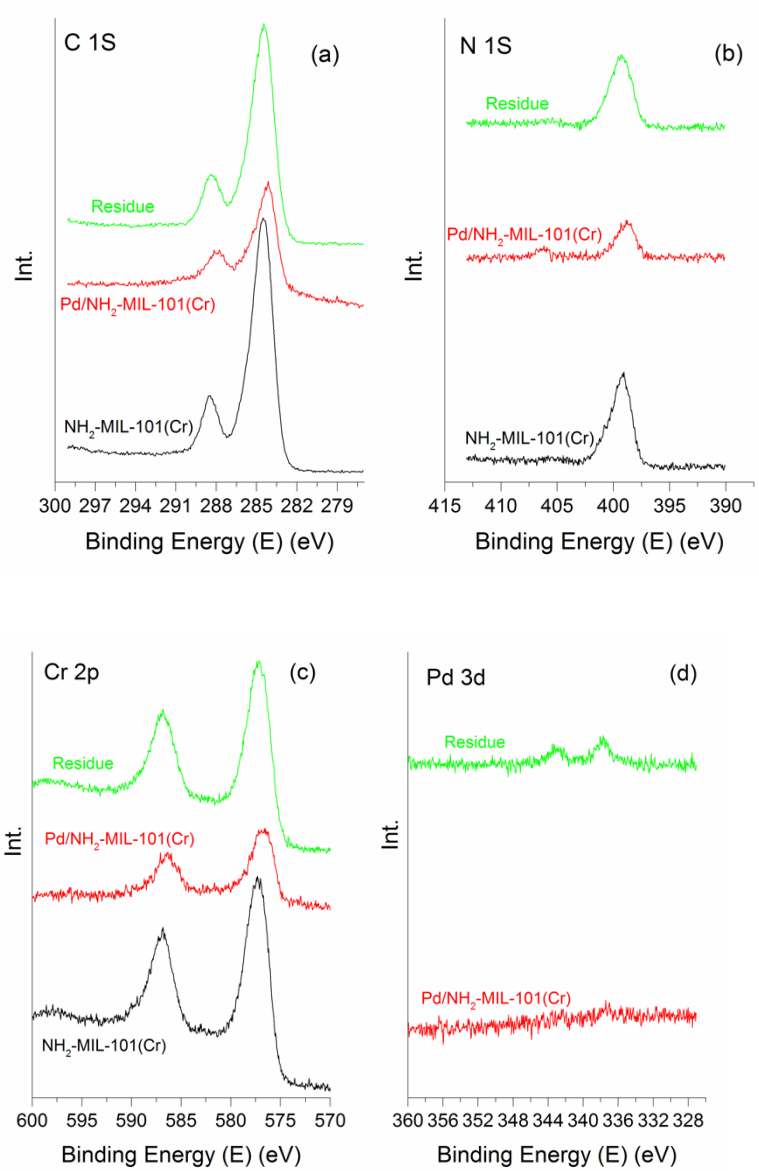

Figure S3. XPS spectra of synthesised NH_2-MIL-101(Cr), Pd/NH_2-MIL-101(Cr) and residual after 6 consecutive reactions.

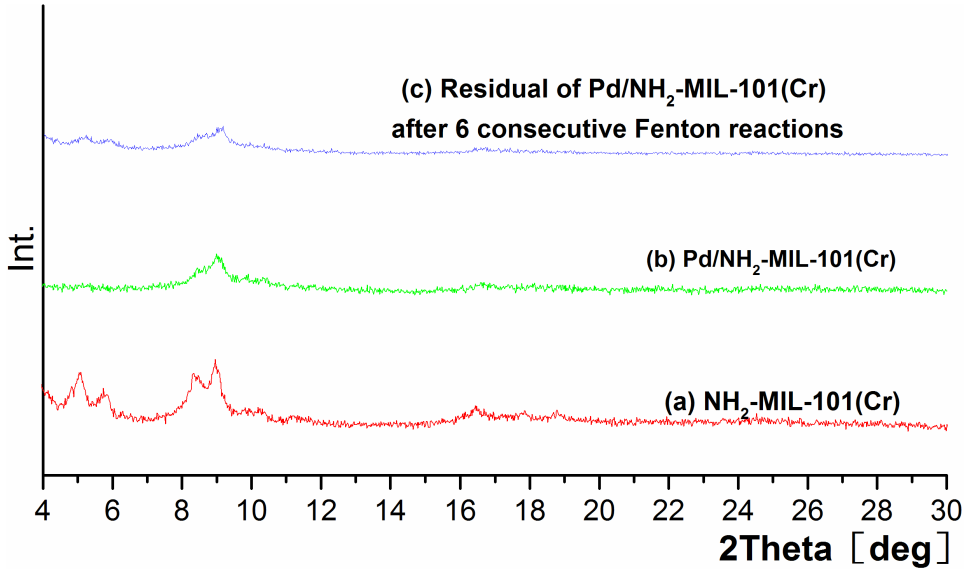

Figure S4. (a) The XRD pattern of NH_2-MIL-101(Cr); (b) the XRD pattern of Pd/NH_2-MIL-101(Cr); (c) the XRD pattern of residual after 6 consecutive reaction cycles.

In summary, it is indicated that NH_2-MIL-101(Cr) was successfully synthesised.

As shown in Figure S5(a), the appearance of the synthesised Pd/NH_2-MIL-101(Cr) is a yellow-green powder. Both of the EDX spectrums shown in Figure S5(b) and the element mappings images shown in Figure S6(g) demonstrated that the C, O, N, Cr, and Pd were distributed in the synthesised material.

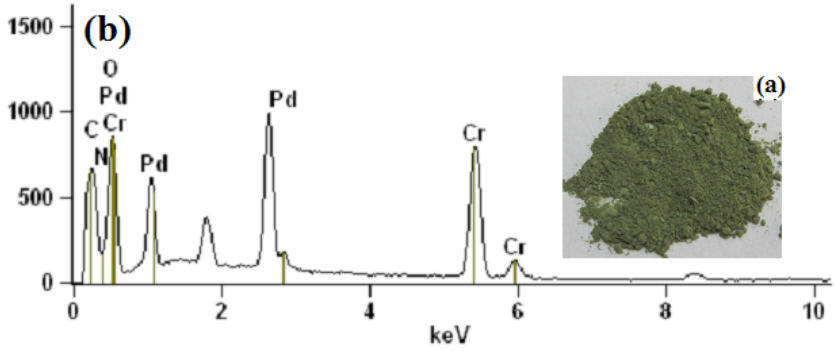

Figure S5. (a) The appearance of Pd/NH_2-MIL-101(Cr); (b) the EDX photograph of Pd/NH_2-MIL-101(Cr).

According to the XPS spectrums of synthesised Pd/NH_2-MIL-101(Cr) shown in Figure S3, the main elements on the surface of this material appeared at the binding energies levels of 284.13 eV (C 1s), 399.18 eV (N 1s), 586.43 eV and 577.23 eV (Cr 2p), and 335.68 eV (Pd 3d), respectively. These results are consistent with previous works on the synthesis of Pd/NH_2-MIL-101(Cr) [7,8]. The signal of Pd was weak. This may be due to the low load content of Pd^0 (only 0.523 wt%) on the surface of this material. Furthermore, according to the TEM images of this material shown in Figures S6(c) to S6(f), the Pd^0 was uniformly dispersed within the abundant cavities. This confirms the successful loading of Pd^0 on the surface of NH_2-MIL-101(Cr). The SEM of this material, exhibited in Figure S6(a) and Figure S6(b) was similar to that of NH_2-MIL-101(Cr) mentioned. And the particle size of this MOFs material did not change significantly.

The specific surface area of this synthesised material was 1001.98 $m^2\ g^{-1}$ measured by BET test. Pd^0 particle occupied the cavities or blocks of outer surfaces of NH_2-MIL-101(Cr). It is consistent with the results obtained by Saikia et al. [7]. The XRD of synthesised Pd/NH_2-MIL-101(Cr), shown in Figure S4, was similar to that reported previously [7,9].

Hence, the results showed that Pd/NH_2-MIL-101(Cr) material was well synthesised in all cases.

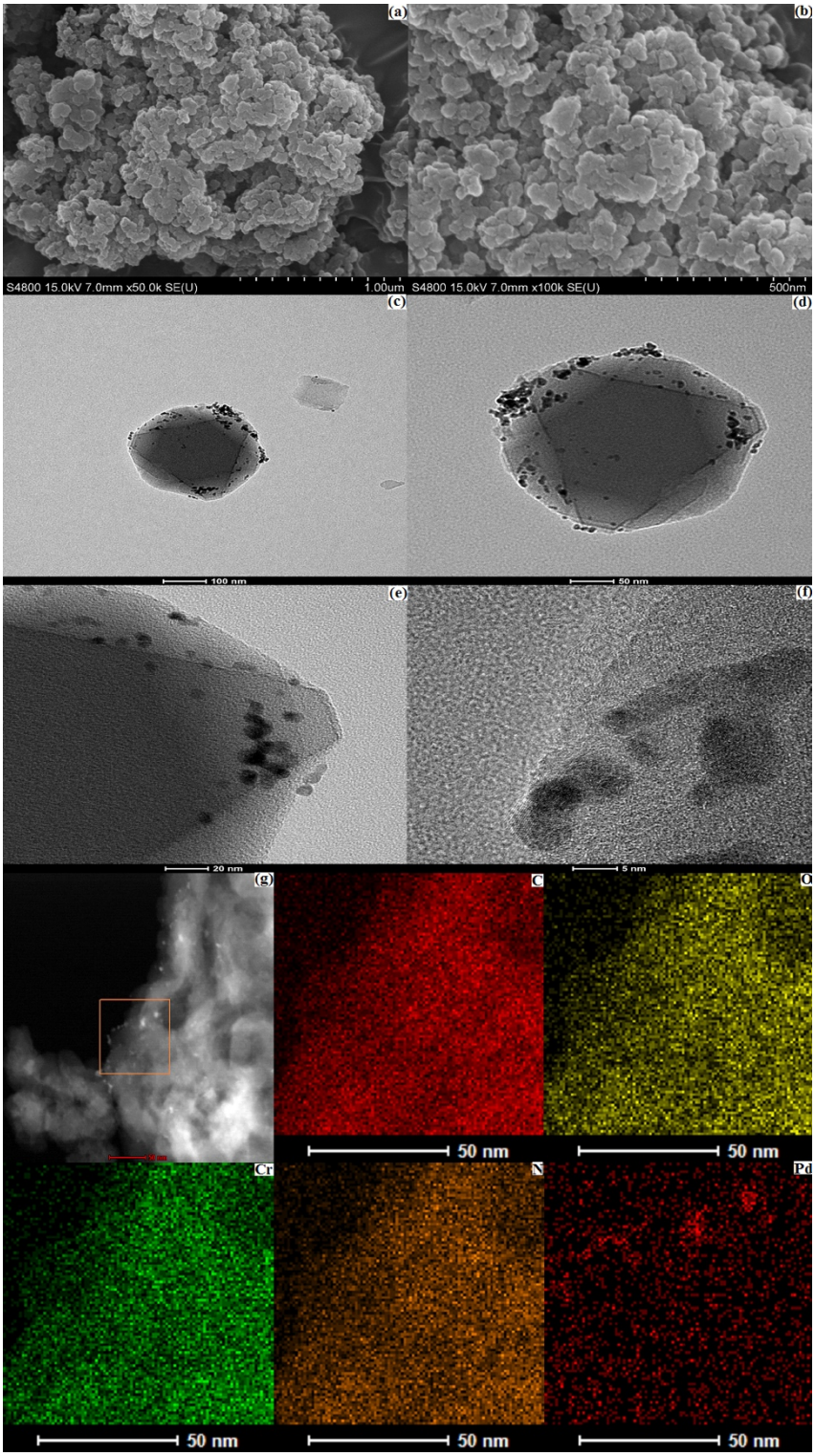

Figure S6. (a) The SEM photograph of Pd/NH_2-MIL-101(Cr) (1 μm scale); (b) the SEM photograph of Pd/NH_2-MIL-101(Cr) (500 nm scale); (c) the TEM photograph of Pd/NH_2-MIL-101(Cr) (200 nm scale); (d) the TEM photograph of Pd/NH_2-MIL-101(Cr) (100 nm scale); (e) the TEM photograph of Pd/NH_2-MIL-101(Cr) (20 nm scale); (f) the TEM

photograph of Pd/NH_2-MIL-101(Cr) (5 nm scale); (g) element mappings images of Pd/NH_2-MIL-101(Cr).

References

1. Modrow A, Zargarani D, Herges R, Stock N. Introducing a photo-switchable azo-functionality inside Cr-MIL-101-NH_2 by covalent post-synthetic modification. Dalton Transactions 2012; 41: 8690-8696.
2. Tian N, Jia Q, Su H, Zhi Y, Ma A et al. The synthesis of mesostructured NH_2-MIL-101(Cr) and kinetic and thermodynamic study in tetracycline aqueous solutions. Journal of Porous Materials 2016; 23: 1269-1278.
3. Li X, Pi Y, Xia Q, Li Z, Xiao J. TiO_2 encapsulated in salicylaldehyde-NH_2-MIL-101 (Cr) for enhanced visible light-driven photodegradation of MB. Applied Catalysis B: Environmental 2016; 191: 192-201.
4. Chong S, Wang T, Cheng L, Lv H., Ji M. Metal-organic framework MIL-101-NH_2-supported acetate-based butylimidazolium ionic liquid as a highly efficient heterogeneous catalyst for the synthesis of 3-aryl-2-oxazolidinones. Langmuir 2018; 35: 495-503.
5. Zhang Y, Li Z, Zhao Q, Zhou Y, Liu H et al. A facilely synthesized amino-functionalized metal–organic framework for highly specific and efficient enrichment of glycopeptides. Chemical Communications 2014; 50: 11504-11506.
6. Luo X, Shen T, Ding L, Zhong W, Luo J et al. Novel thymine-functionalized MIL-101 prepared by post-synthesis and enhanced removal of Hg^{2+} from water. Journal of hazardous materials 2016; 306: 313-322.
7. Saikia M, Kaichev V, Saikia L. Gold nanoparticles supported on nanoscale amine-functionalized MIL-101(Cr) as a highly active catalyst for epoxidation of styrene. RSC advances 2016; 6: 106856-106865.

8. Luo X, Ding L, Luo J. Adsorptive removal of Pb (II) ions from aqueous samples with amino-functionalization of metal–organic frameworks MIL-101(Cr). Journal of Chemical & Engineering Data 2015; 60: 1732-1743.

9. Carson F, Pascanu V, Bermejo G, Zhang Y, Platero-Prats A et al. Influence of the base on Pd@ MIL-101-NH_2 (Cr) as catalyst for the suzuki-miyaura cross-coupling reaction. Chemistry-A European Journal 2015; 21: 10896-10902.